Astron. Astrophys. 356, 627–642 (2000)

ASTRONOMY AND ASTROPHYSICS

Twin X-ray flares and the active corona of AB Dor observed with *Beppo*SAX

A. Maggio[1], **R. Pallavicini**[1], **F. Reale**[2], **and G. Tagliaferri**[3]

[1] Osservatorio Astronomico di Palermo, Palazzo dei Normanni, 90134 Palermo, Italy
[2] Dipartimento Scienze Fisiche e Astronomiche, Università Palermo, Sezione di Astronomia, Piazza del Parlamento 1, 90134 Palermo, Italy
[3] Osservatorio Astronomico di Brera, Via E. Bianchi 46, 23807 Merate (LC), Italy

Received 25 October 1999 / Accepted 25 January 2000

Abstract. We present two X-ray observations of the young, active star AB Dor, performed with *Beppo*SAX on Nov 9 and Nov 29 1997, and lasting 50 ksec and 140 ksec, respectively. Two, quite similar, large flares occurred during these observations, characterized by a 100-fold increase of the X-ray flux, peak temperatures of about 10^8 K, and peak emission measures of $\sim 5 \times 10^{54}$ cm^{-3}.

We have performed a detailed, time-resolved analysis of the LECS and MECS X-ray spectra during the flares, and also in the subsequent quiescent phases. We have derived a metal abundance of the coronal plasma about half the photospheric one, with no significant increase during the flaring events. However, abundance variations of less than a factor ~ 3 cannot be excluded, within our statistical uncertainties. The exponential decay of the X-ray light curves, and the time evolution of plasma temperature and emission measure are similar to those observed in compact solar flares. The analysis of the flare decay, following the method of Reale et al. (1997), indicates the presence of sustained heating, and yields coronal loop maximum heights smaller than (but comparable with) the stellar radius, in both cases.

The flares occurred at different rotation phases, and in one case, the decay was observed for one entire rotation period with no evidence of self-eclipse by the star. We conclude that the flaring loops may be located in the circumpolar region of AB Dor, but they do not appear to be related in any way with the large magnetic structures which sustain the well-known prominences of AB Dor, at several stellar radii above the surface.

During the quiescent phase, lasting two rotation periods after the second flare, we have found evidence of significant low-level variability but no indication of rotational modulation. This variability, together with the high plasma temperature (~ 25 MK) and large emission measure ($\lesssim 10^{53}$ cm^{-3}), are interpreted in the framework of a saturated corona.

Key words: stars: coronae – stars: late-type – stars: abundances – stars: activity – X-rays: stars – stars: individual: AB Dor

Send offprint requests to: (maggio@oapa.astropa.unipa.it)

1. Introduction

AB Doradus (HD 36705, spectral type K0–K1 V) is one of the most interesting, and most intensively studied, coronal X-ray sources. It is one of the most rapidly rotating single stars known, with a period of only 12.4 hours, and it is relatively close, at $\approx$ 15 pc. Furthermore, it is a very young star with a strong lithium absorption line and kinematic properties characteristic of the Pleiades moving group. These properties make it probably the nearest ZAMS star known, with an age of $\approx$ 20–30 million years (Collier-Cameron & Foing 1997), and an easy-to-study analog of the numerous rapidly rotating K dwarfs in the Pleiades open cluster and in star forming regions, which are all at much larger distances.

AB Dor was first detected in X-rays by the *Einstein* Observatory (Pakull 1981; Vilhu & Linsky 1987) and later re-observed with EXOSAT (Collier-Cameron et al. 1988), GINGA (Vilhu et al. 1993), ROSAT (Kürster et al. 1997), and ASCA (White et al. 1996; Mewe et al. 1996; Ortolani et al. 1998). EUV/FUV spectroscopic observations were also performed with EUVE (simultaneously with ASCA; Rucinski et al. 1995; Mewe et al. 1996), and with ORFEUS (simultaneously with ROSAT; Schmitt et al. 1997, 1998).

The coronal emission of AB Dor is characterized by high-level variability on time scales from minutes to weeks (Kürster et al. 1997). Flares have been frequently detected, with an average rate of two per day (i.e. one per rotation cycle) estimated by Vilhu et al. (1993). From ASCA and EUVE observations, Mewe et al. (1996) and Ortolani et al. (1998) derived a coronal metallicity $Z \sim 0.3 Z_\odot$ in the quiescent state, while a nearly solar photospheric abundance was derived by Vilhu et al. (1987) by means of spectroscopic observations with the CAT/CES telescope at the European Southern Observatory.

UV observations with IUE were reported by Rucinski (1985) and by Collier Cameron et al. (1990), and with the Goddard High-Resolution Spectrograph (GHRS) on the Hubble Space Telescope (HST) by Vilhu et al. (1998). The chromospheric and transition region emission of AB Dor, as well as its coronal emission, are all close to the empirical saturation level defined by the most rapid rotators and young stars (Vilhu 1984; Vilhu & Walter 1987), which emit at UV/X-ray wavelengths about 10^{-3} of their bolometric luminosity.

Many optical observation campaigns of AB Dor provide us with long-term monitoring of the photospheric emission (see Innis et al. 1988 and Kürster et al. 1997 for a summary of available V-band data), and of the circumstellar system of cool (8–9 $\times 10^3$ K) clouds, or prominence-like condensations, revealed by transient absorption features in the Hα line (Collier-Cameron & Robinson 1989a; Collier-Cameron & Robinson 1989b;
Collier-Cameron et al. 1990).

Optical photometry shows a stable and clearly modulated light curve, persisting since its discovery in 1980 (Pakull 1981), explained by large and long-lived starspots. Most recently, mapping of the photospheric spot distribution on AB Dor was achieved by means of high-resolution optical spectra and Doppler imaging techniques (Kürster et al. 1994; Collier-Cameron & Unruh 1994; Collier-Cameron 1995; Unruh et al. 1995). At any time, the photosphere of AB Dor appears to be covered by dark spots, with a total surface filling factor of 10–20%.

The wealth of data available suggests that the outer atmosphere of AB Dor is permeated by a multitude of magnetic structures with a complex topology (Donati & Collier-Cameron 1997; Donati et al. 1999). The largest ones should extend to heights of several times the stellar radius, in order to support the prominences in a state of enforced co-rotation, as inferred from the Hα observations. What is presently not clear is whether such large coronal structures are important contributors to the quiescent and/or flaring X-ray emission of AB Dor. In particular, we do not know whether the flaring activity originates from coronal structures preferentially located at some active longitudes and in the low-latitude ($< 30^\circ$) activity belts suggested by the Doppler images (Kürster et al. 1994; Unruh et al. 1995), or at some higher latitudes ($\gtrsim 60^\circ$), where short-lived starspots have been observed (Unruh et al. 1995) and the magnetic structures supporting the slingshot prominences are presumed to be located (Donati & Collier-Cameron 1997). A related question is whether and how the surface magnetic activity influences the number and the dynamics of the clouds corotating with the hot corona, e.g. via solar-like coronal mass ejections.

In this paper we report the analysis of a *Beppo*SAX observation of AB Dor, in which two apparently identical flares occurred, actually the largest X-ray flares ever recorded from AB Dor. We will focus our attention on the time-resolved spectral analysis of the X-ray emission detected with the Low-Energy and Medium-Energy Concentrator Spectrometers (LECS and MECS); a companion paper by Pallavicini et al. (in preparation) is devoted to the analysis of the hard X-ray emission (> 10 keV), detected with the High-Pressure Gas Scintillation Proportional Counter (HPGSPC) and with the Phoswich Detector System (PDS) (see an early report in Pallavicini & Tagliaferri 1999). The scope of our work is to study the thermodynamic properties and the metal abundance of the plasma in the flaring and quiescent corona of AB Dor; moreover, the analysis of the flare decay is employed to constrain the physical parameters of the flaring region, including its geometry and location on the star.

In Sect. 2 we present a critical assessment of some of the stellar parameters required for the interpretation of the data; the *Beppo*SAX observations are described in Sect. 3; the results of the analysis are presented in Sect. 4 and in Sect. 5, and discussed in Sect. 6; Sect. 7 is devoted to a summary and final conclusions.

2. Stellar parameters

The most recent determination of the parallax of AB Dor, $\pi =$ 66.3–67.2 mas, derived from precise VLBI (Very Long Baseline Interferometry) astrometric measurements by Guirado et al. (1997), is in perfect agreement with the value derived from the *Hipparcos* data (ESA 1997) of 66.92 ± 0.54 mas.

A reliable estimate of the radius of AB Dor is very desirable for a comparison with the scale height of the coronal structures, while the inclination of its rotation axis with respect to the line of sight is required to study the visibility of these regions at different rotation phases. Unfortunately, there are still large uncertainties on both parameters (see Appendix A). In the following, we will assume a stellar radius of 1.0 $R_\odot$, a mass of $0.76 M_\odot$, and an inclination $i = 60^\circ$, consistently with the classification of AB Dor as a K1 dwarf of age 20–30 Myr, in the final phases of contraction onto the main-sequence (Collier Cameron & Foing 1997; Appendix A). Its young age remains strongly indicated by the high lithium abundance, $\log \epsilon$(Li) = 3.1 (Vilhu et al. 1987; Vilhu et al. 1991; Randich et al. 1993), by the membership in the Pleiades moving group (Innis et al. 1985), and by the short rotation period ($P_{\rm rot} = 0.514$ days; Pakull 1981; Innis et al. 1988).

Assuming $m_{\rm v} = 6.76$ and $B - V = 0.80$ for AB Dor unspotted[1], we get $\log T_{\rm eff} = 3.72$ and $BC = -0.20$ using the transformations by Flower (1996), and hence we derive a bolometric luminosity of 1.58×10^{33} erg s^{-1}.

In order to trace the rotation cycles of AB Dor during the *Beppo*SAX observations, we have adopted the ephemeris by Innis et al. (1988):

$$\mathrm{HJD} = 2\,444\,296.575 + 0.51479E \qquad (1)$$

with the phase $\phi = 0$ corresponding to the passage of spot "A" of Innis et al. on the central meridian of the visible hemisphere.

Finally, AB Dor has an apparent physical companion at about $10''$ separation, the dM4e flare star Rossiter 137B (Lim 1993), which is also a coronal source, with an X-ray luminosity a factor ~ 60 lower than AB Dor quiescent (Vilhu & Linsky 1987). This companion cannot be spatially resolved by SAX observations, but it does not contaminate significantly the X-ray spectrum of AB Dor. A third low-mass (0.08–0.11 $M_\odot$) companion orbiting AB Dor was recently found by Guirado et al. (1997), with a separation of $0.2''$–$0.7''$ (3–10 AU). Lacking any further information on its nature, we have assumed a negligible contamination in X-rays, also in this case.

[1] the values of $m_{\rm v}$ and $B - V$ assumed here refer to the epoch of the maximum brightness, when AB Dor was in fact the least spotted (see Appendix A).

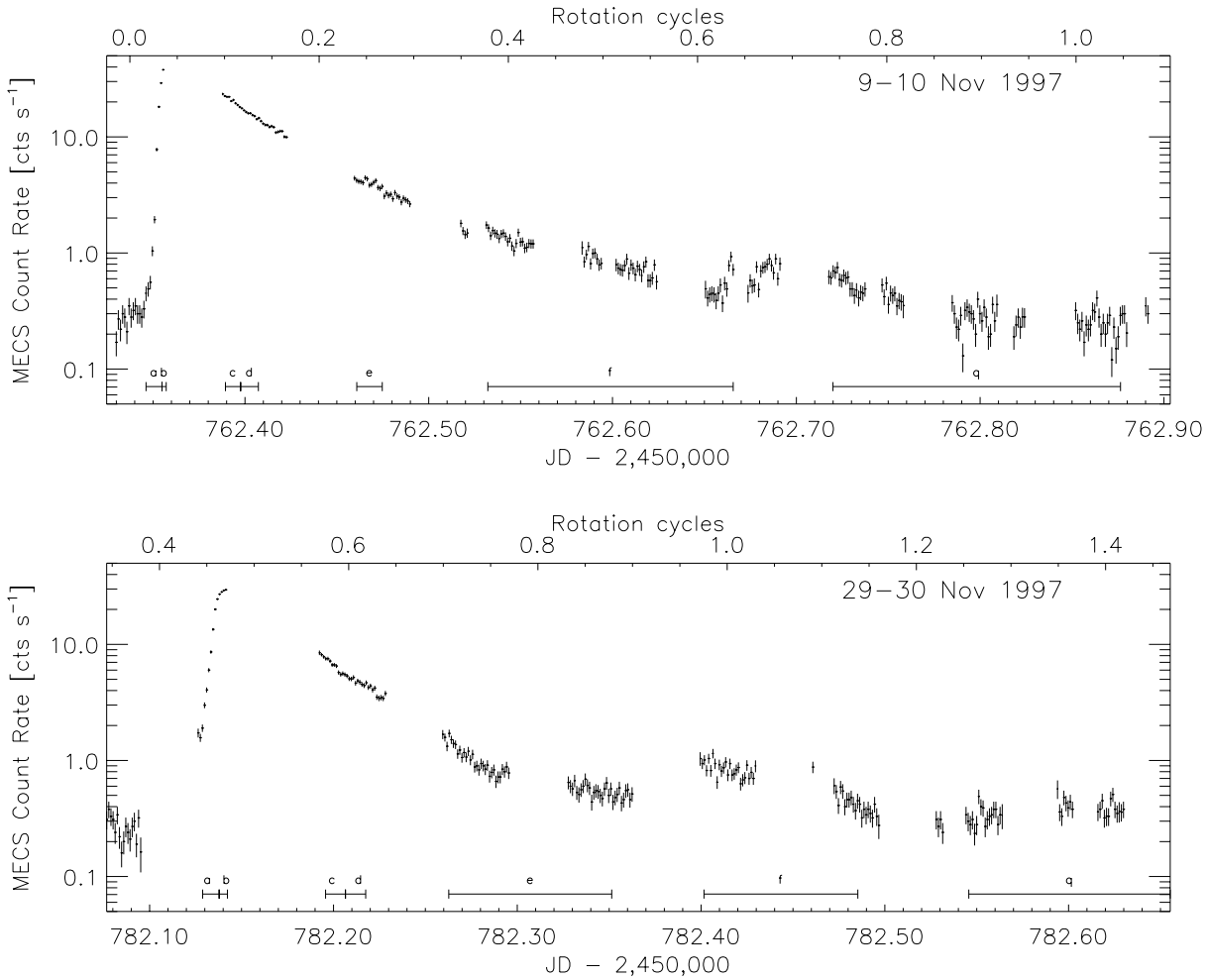

Fig. 1. SAX/MECS X-ray light curves of AB Dor in the 1–10 keV band, binned into 100 sec intervals, plotted vs. Julian days (bottom axis) and rotation cycles (top axis). The letters at the bottom mark the time segments where spectra have been accumulated (Table 1). Note that the Nov 29 light curve has been truncated so to have the same duration (50 ksec) of the Nov 9 observation; the segment labeled *q* covers only part of the entire "quiescent" time segment, more clearly shown in Fig. 4.

3. The *Beppo*SAX observations

The SAX observation of AB Dor started on Nov. 9, 1997 at 19:47 UT, but it was interrupted for technical reasons on Nov. 10 at 9:56, after 50 ksec of elapsed time, i.e. slightly more than one full rotational cycle. The observation was then resumed three weeks later, on Nov. 29 at 13:49, and completed after 140 ksec of elapsed time, on Dec. 1 at 4:53 UT, corresponding to three rotational cycles.

Strikingly enough, two huge flares started just at the beginning of both observation segments, as documented by the X-ray light curves in Fig. 1. In the same figure we have reported the rotation cycles of AB Dor, computed according to the ephemeris by Innis et al. (1988). Given the large count rates, we were able to perform a detailed time-resolved spectral analysis of the data, in both cases.

For the analysis of the LECS and MECS data, we have adopted the standard cleaned and linearized event files provided by the *Beppo*SAX Science Data Center, from which light curves and spectra were extracted. The total exposure times were of 12.1 ksec and 25.2 ksec, for the LECS and the MECS respectively, in the first observation, and of 31.1 ksec and 61.6 ksec, in the second observation.

Given the relatively high absolute galactic latitude of AB Dor ($b = -33°$), the cosmic X-ray background spectra were accumulated, for each detector, from the relevant "blank fields" event files. We have checked that – in the worst case, i.e. for the quiescent spectrum – the background is not negligible only for energies > 7 keV for the LECS, and > 8 keV for the MECS, given the high intensity of the source.

4. Data analysis and results

The 9 Nov flare was slightly more intense than the flare on Nov 29, showing higher maximum count rates (Fig. 2). Unfortunately, the LECS was not active during the rise phase of the Nov 9 flare, and also the MECS data do not include the peak of the flare, at variance from the Nov 29 flare.

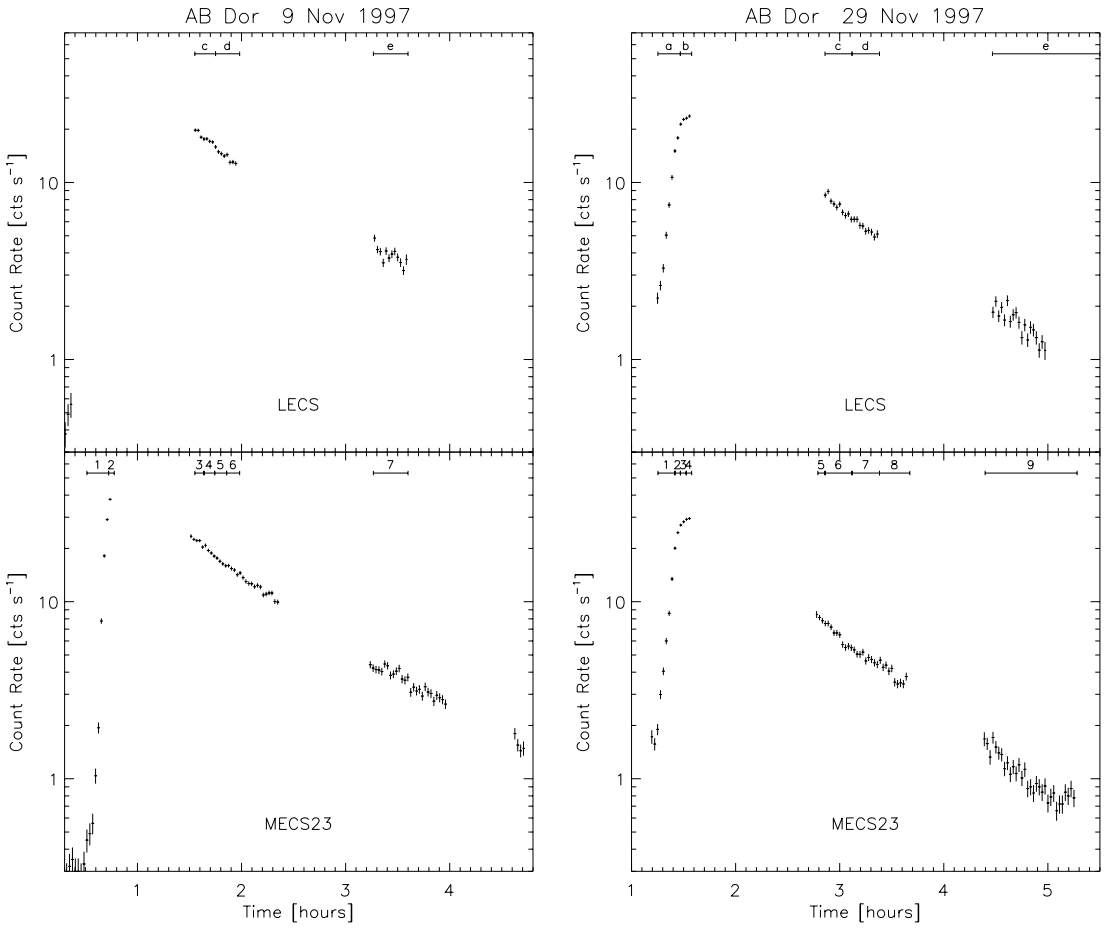

Fig. 2. LECS and MECS X-ray light curves of AB Dor over a time span of four hours and a half, covering the two flares occurred on 9th and 29th Nov, 1997 (times are measured from the beginning of each observation). The letters on top of the upper (LECS) panel mark some of the time segments already shown in Fig. 1, where spectral analysis of LECS and MECS spectra has been performed with 2-T models (Sect. 4.2). Instead, on top of the lower (MECS23) panel are indicated the time segments chosen for the 1-T model fitting of the MECS spectra only (Sect. 4.3).

In order to perform a time-resolved spectral analysis, we have divided each observation in a number of time segments (Fig. 2), so to get between 2000 and 6000 source counts in each extracted spectrum. These spectra have been re-binned so to sample the instrument resolution with 3 bins at all energies, thus increasing the S/N ratio per bin and ensuring a uniform oversampling of the redistribution matrix, at the same time.

We have used XSPEC V10.00 to fit the LECS and MECS spectra in the energy ranges 0.12–4 keV and 1.8–10 keV, respectively, using χ^2 statistics with weights evaluated according to Gehrels (1986). For the spectral fitting we have employed multi-component thermal models, adopting the MEKAL emissivities for an optically-thin plasma in collisional equilibrium, computed by Mewe et al. (1985; 1986), based on the ionization balance of Arnaud & Raymond (1992) for iron. The reference element abundances of the coronal plasma are the solar system ones of Anders and Grevesse (1989), and in particular the adopted Fe abundance is 7.67 (in a log scale, where the H abundance is 12.00).

We have performed the analysis with the following approach: first, we have studied the temporal and spectral characteristics of the X-ray emission during the quiescent phases, and we have evaluated how different fitting model parameters are correlated; second, we have adopted a two-component thermal model to fit the LECS and MECS spectra simultaneously, for each of the selected time segments, in order to study the time evolution of relevant plasma properties, such as the temperature and emission measure of each component, and the plasma metal abundance, during the flares; finally, we have fitted the MECS spectra alone with a single isothermal model, in order to derive effective (average) temperatures and emission measures, and to get an alternative estimate of the plasma metal abundance. A sample of the observed spectra and best-fit 2-T models is displayed in Fig. 3.

While fitting the LECS and MECS spectra jointly, the LECS/MECS cross-calibration factor was not treated as an additional free parameter: after having checked that, in our case, the best-fit value would always fall between 0.71 and 0.85, we have decided to keep its value fixed to 0.77, for all the fits discussed in the following.

4.1. Quiescent emission

The quiescent emission spectra have been extracted from the last of the time segments, labeled q, in each observation (Fig. 1). On Nov 9, the net source count rate in the quiescent segment, lasting ~ 0.3 rotation cycles (elapsed time), was $0.52\,\mathrm{cts\,s^{-1}}$ in the LECS (0.1-4 keV band) and $0.25\,\mathrm{cts\,s^{-1}}$ in the MECS23 (1.8-8 keV band), with live times of 6.1 ksec and 11.8 ksec, respectively. On Nov 29, the quiescent phase was followed instead

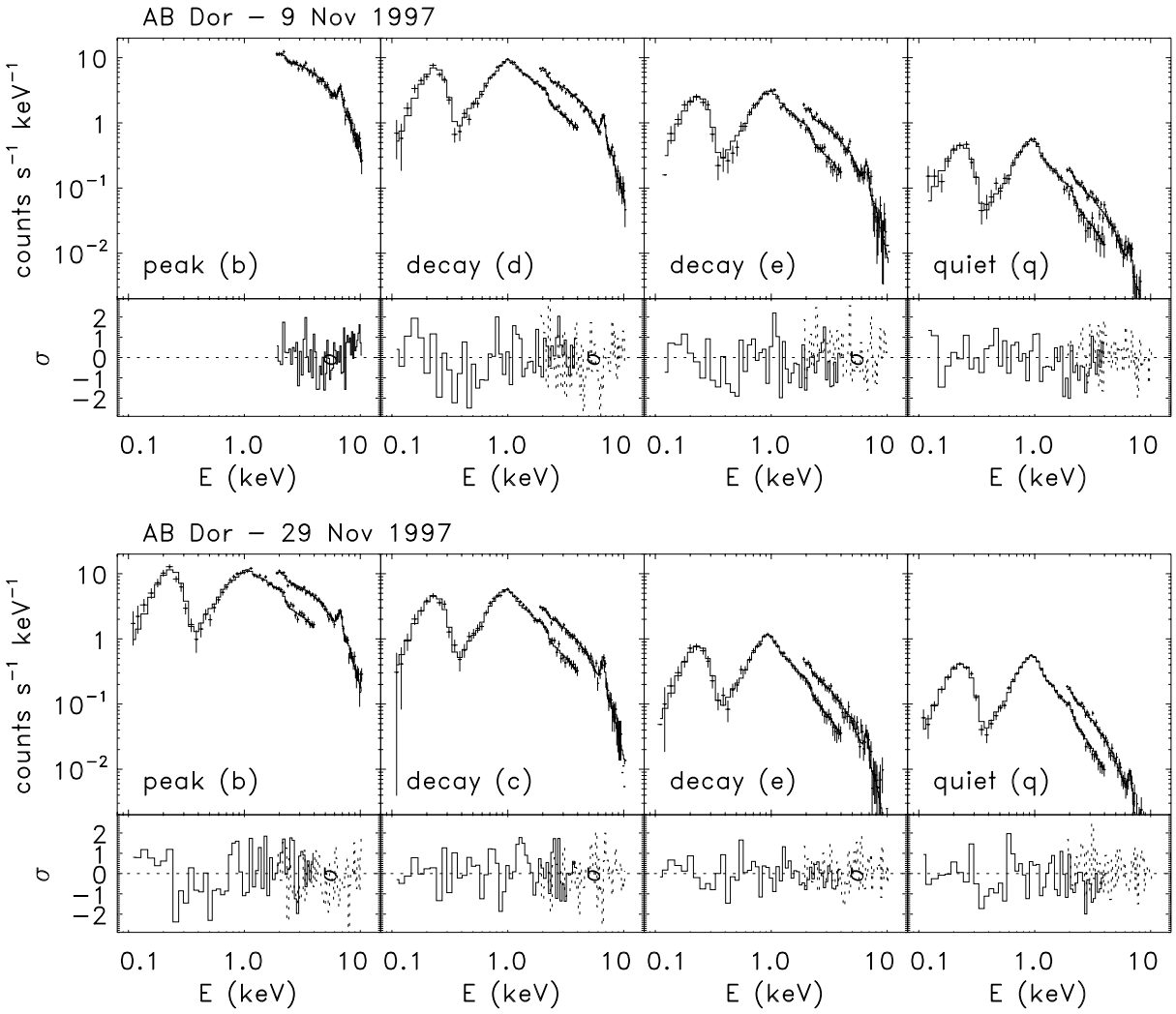

Fig. 3. Sample of SAX LECS and MECS spectra of AB Dor together with best-fit 2-T MEKAL models with variable plasma metallicity, and including variable ISM absorption. The residuals, divided by the statistical error on each data point, are also shown in the lower panels. Note that LECS data are missing at the time of the 9 Nov flare peak. The spectra are marked as in Table 1

for ~ 2.3 rotation cycles, but the mean count rates are similar to the above ones: 0.49 cts s^{-1} in the LECS (22.1 ksec live time) and 0.21 cts s^{-1} in the MECS23 (22.5 ksec live time). The similarity of the count rates and of the spectra analyzed (see below) suggests that the quiescent phases selected on the two dates are both representative of the pre-flare state of AB Dor. However, we have eventually preferred the Nov 29 observation – which is the longer one – for discussing the quiescent coronal properties of AB Dor.

Even during the long quiescent phase after the Nov 29 flare, the coronal emission level of AB Dor is far from being constant (Fig. 4): in fact, significant low-level variability is clearly present, as testified by the short-term fluctuations of both the count rate and the hardness ratio (defined as the ratio of the count rates in the energy bands 0.1–1.8 keV and 1.8–8 keV). In particular, the count rates show a scatter (standard deviation) of 21% around the mean value for the LECS, and of 24% for the MECS; the reduced χ^2, computed against the hypothesis of a constant source, is 5.5 with 31 d.o.f. for the LECS, and 4.7 with 80 d.o.f. for the MECS. A detailed timing analysis of the X-ray light curve of AB Dor in quiescent state is beyond the scope of the present paper, but no apparent correspondence is visible between the variations of the count rate and the rotation phases of AB Dor.

In order to get a good-quality fit of the quiescent spectra, at least two thermal components are required, including the metal abundance (equal for the two components) as a free parameter. We have first performed a joint fit of the LECS and MECS spectra, on each of the two dates, keeping the hydrogen column density, $N_{\rm H}$, fixed to 2×10^{18} cm^{-2}, i.e. to the value derived by Mewe et al. (1996) from the analysis of EUVE data. The resulting best-fit parameters are the following: on Nov 9, the two components have temperatures of 9^{+1}_{-2} MK and 29^{+6}_{-4} MK, with a ratio of the emission measures $EM_1/EM_2 = 0.6$, and the plasma metallicity is $Z = 0.4^{+0.2}_{-0.1}$ solar; on Nov 29, we have obtained temperatures of $8.1^{+0.9}_{-0.6}$ MK and 23^{+2}_{-1} MK, with

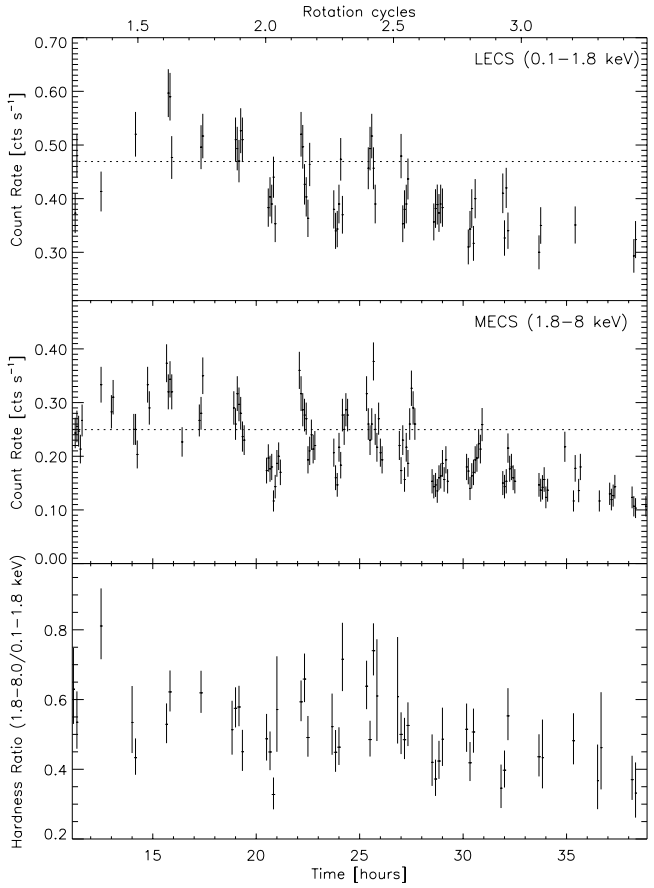

Fig. 4. LECS and MECS X-ray light curves and hardness ratio of AB Dor in the post-flare quiescent state, on Nov 29. The dotted lines indicate the mean count rates in the present time interval. Bins of 5 min have been used for the light curves, while the hardness ratio has been computed in bins of 10 min and where both the LECS and MECS data are available.

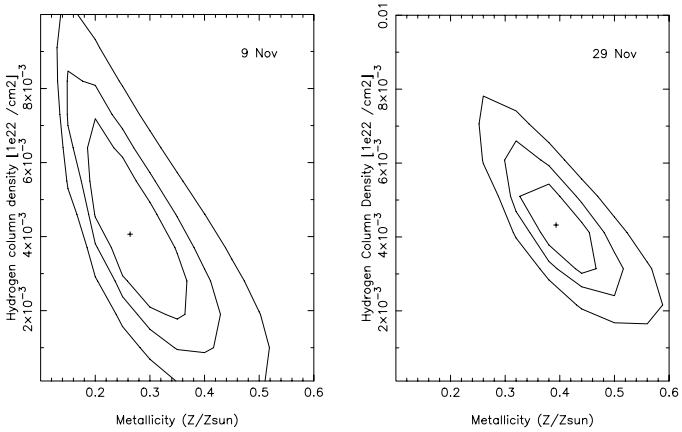

Fig. 5. Contour map of χ^2 values in the $N_{\rm H}$ vs. $Z/Z_{\odot}$ parameter plane. The plus marks the 2-T model best-fitting the LECS and MECS spectra during the AB Dor quiescent phase. The three contours correspond to the 68%, 90%, and 99% confidence levels, for the two interesting parameters. Note the anticorrelation between hydrogen column density and metallicity.

$EM_1/EM_2 = 0.3$, and $Z = 0.6 \pm 0.1$. Overall, the corona of AB Dor appears slightly hotter on Nov 9 than on Nov 29.

Although the χ^2 of the above fits is formally acceptable, a systematic overprediction of the counts observed at energies < 0.3 keV suggests an hydrogen column density larger than assumed, which could be justified by absorption in the circumstellar environment (Sect. 6). In fact, if also this parameter is left free to vary, fits of even better quality are obtained, having $N_{\rm H} \approx 4 \times 10^{19}$ cm^{-2} (see Table 1). The best-fit temperatures are similar to the above ones, while somewhat lower metal abundances, 0.3–0.4 solar, and emission measure ratios higher by factors 1.5–2 have been obtained on Nov 9 and Nov 29, respectively.

Since allowing the hydrogen column density to vary yields, in general, fits of better quality, we have followed the same approach also in the analysis of the spectra taken during the flares. However, we stress that a correlation is present between the metallicity and the hydrogen column density, as it is clearly evident from the statistical confidence regions in the plane of these two parameters, shown in Fig. 5. A similar cross-talk between different model parameters, and in particular between metallicity and emission measure ratio, has been already discussed by Favata et al. (1997).

4.2. 2-T fits of LECS and MECS flare spectra

We have extracted spectra in 6 time segments (*a–f* in Table 1) covering each of the two flares. The average MECS count rates in the "peak" segments are about 120 times larger than in the quiescent phase, and they remain more than 10 times larger than the quiescent level for about two hours and a half after the peak (see Table 2 in Sect. 4.3). Hence, most of the extracted spectra are dominated by the flaring plasma emission, with a negligible contribution from the rest of the quiescent coronal plasma in the visible hemisphere. Only in the last two time segments, 30% and 50% of the observed count rate, respectively, can be attributed to emission from plasma outside the flaring region.

A 2-T model has been adopted to fit the LECS and MECS23 joint pairs of spectra, except for the rise and peak segments of the 9 Nov flare, where LECS data are not available and a 1-T model was sufficient for the fitting. We have obtained acceptable fits (probability $> 10\%$) in all cases (Table 1), with the exception of the segment d on Nov 9. In some cases, a satisfactory fit could be obtained also with $N_{\rm H}$ fixed to the low value (2×10^{18} cm^{-2}) derived from EUV data (Mewe et al. 1996), but for the time segments c, d, and e on Nov 29, and a, b, and c on Nov 9, the resulting χ^2 values are definitely not acceptable (at the 99% confidence level) if such a low H column density is assumed.

The variations of the temperatures, emission measures, metal abundance, and H column density vs. time are shown in Fig. 6. On Nov 9, we find a temperature of ≈ 100 MK in the "peak" segment, which actually precedes the true flare peak, corresponding to an increase by a factor ~ 4 with respect to the temperature of the hotter component in the quiescent phase, accompanied by a factor ~ 50 increase of the emission measure, which reaches the maximum value of $\sim 4 \times 10^{54}$ cm^{-3} at the

Table 1. Two-temperature model fitting[a] of the AB Dor LECS + MECS spectra.

Bin ID	Source State	$N_{\rm H}$ 10^{19} cm^{-2}	$Z/Z_\odot$ [b]	T_1 10^6 K	EM_1/EM_2	T_2 10^6 K	$EM_2/10^{52}$ cm^{-3}	$f_{\rm x}/10^{-11}$ [c] erg cm^{-2} s^{-1}	$\chi^2_{\rm r}$	d.o.f.
				9 Nov						
q	quiet	0.2[d]	$0.4^{+0.1}_{-0.1}$	$9.3^{+0.8}_{-1.2}$	0.55	$29.2^{+4.3}_{-3.0}$	8.8	7.6	0.83	85
q	quiet	$4.1^{+5.2}_{-4.0}$	$0.3^{+0.2}_{-0.1}$	$9.5^{+1.0}_{-1.3}$	0.94	$31.8^{+10.9}_{-5.1}$	8.3	8.0	0.79	84
a	rise	0.2[d]	$0.5^{+0.2}_{-0.2}$			$95.4^{+15.9}_{-12.1}$	96.2	71.4	0.76	56
b	peak	0.2[d]	$0.7^{+0.2}_{-0.1}$			$109.2^{+17.6}_{-10.8}$	561.2	441.7	0.82	56
c	decay	$6.6^{+2.0}_{-1.8}$	$0.5^{+0.1}_{-0.1}$	$15.9^{+3.7}_{-2.6}$	0.44	$71.5^{+19.8}_{-11.1}$	318.0	298.6	1.07	101
d	decay	$8.6^{+2.2}_{-2.0}$	$0.5^{+0.1}_{-0.1}$	$12.6^{+3.4}_{-1.9}$	0.20	$53.9^{+11.7}_{-4.8}$	296.6	230.8	1.31	102
e	decay	$5.0^{+3.3}_{-2.8}$	$0.4^{+0.2}_{-0.2}$	$9.9^{+2.3}_{-1.6}$	0.22	$39.1^{+7.7}_{-4.1}$	84.2	61.5	0.97	89
f	decay	$6.6^{+5.3}_{-4.2}$	$0.3^{+0.3}_{-0.2}$	$9.6^{+2.2}_{-2.0}$	0.36	$30.4^{+9.6}_{-3.8}$	22.5	16.3	0.73	84
				29 Nov						
q	quiet	0.2[d]	$0.6^{+0.1}_{-0.1}$	$8.1^{+0.7}_{-0.3}$	0.34	$22.6^{+1.2}_{-0.8}$	8.2	6.9	0.95	90
q	quiet	$4.4^{+2.4}_{-2.2}$	$0.4^{+0.1}_{-0.1}$	$8.8^{+0.7}_{-0.8}$	0.55	$23.1^{+2.2}_{-1.5}$	8.8	7.2	0.73	89
a	rise	$6.1^{+3.1}_{-2.6}$	$0.6^{+0.2}_{-0.2}$	$15.8^{+4.6}_{-3.1}$	0.25	$110.4^{+52.9}_{-24.5}$	152.3	138.7	0.93	89
b	peak	$6.2^{+2.5}_{-2.1}$	$0.6^{+0.4}_{-0.2}$	$20.1^{+25.8}_{-8.2}$	0.23	$85.5_{-16.9}$	438.3	385.0	1.17	95
c	decay	$5.9^{+2.7}_{-2.3}$	$0.6^{+0.2}_{-0.2}$	$9.4^{+1.7}_{-1.5}$	0.18	$37.6^{+3.9}_{-3.1}$	149.7	111.9	0.99	89
d	decay	$4.6^{+3.1}_{-2.7}$	$0.8^{+0.3}_{-0.2}$	$10.0^{+1.9}_{-1.4}$	0.17	$35.4^{+5.0}_{-2.9}$	105.6	83.5	0.74	89
e	decay	$9.9^{+7.2}_{-4.6}$	$0.3^{+0.2}_{-0.2}$	$9.4^{+1.3}_{-1.4}$	0.63	$30.7^{+13.9}_{-4.2}$	21.5	18.0	0.53	85
f	decay	$1.6^{+4.9}_{-1.5}$	$0.6^{+0.4}_{-0.3}$	$7.7^{+2.3}_{-2.0}$	0.20	$31.1^{+6.8}_{-3.5}$	17.0	12.9	0.93	85

[a] The 68% joint confidence ranges have been computed with the criterium $\chi^2 < \chi^2_{min} + \Delta$ (Lampton et al. 1976), where Δ has been chosen according to the actual number of parameters for which errors have been determined, in each case.
[b] Abundances relative to solar system values, with Fe = 7.67 (in logarithmic units, with H = 12.00).
[c] X-ray fluxes, at the source, in the 0.1–10 keV band.
[d] Spectral fitting results obtained with hydrogen column density fixed to $N_{\rm H} = 2 \times 10^{18}$ cm^{-2}. The Nov 9 a and b spectra have been fitted with a 1-T model because only MECS data were available (see text).

same time. On Nov 29, the temperature and emission measure of the hotter component reach values almost identical to the above ones, but the temperature peaks earlier than the emission measure (see also Sect. 4.3), likely because the flare peak was fully covered by the observation; moreover, the cooler component shows an increase of the temperature by a factor ~ 2, up to 20 MK, and an increase of the emission measure by a factor ~ 20, up to $\sim 1 \times 10^{54}$ cm^{-3}, with respect to the corresponding quiescent values.

We find that the best-fit metal abundance reaches values about two times larger than those in quiescent state, but the statistical uncertainties (due in part to the anti-correlation with the H column density) do not allow us to claim, at this stage, that the metallicity variation is significant; this conclusion will be confirmed, with more confidence, in the next section. In a similar fashion, the variations of the best-fit $N_{\rm H}$ value by factors $\gtrsim 2$ are within the statistical errors at the 90% confidence level.

The (unabsorbed) X-ray fluxes, in the 0.1-10 keV band, increase from $\sim 7 \times 10^{-11}$ erg cm^{-2} s^{-1} in quiescence to $\sim 4.4 \times 10^{-9}$ erg cm^{-2} s^{-1} on Nov 9, and to 3.9×10^{-9} erg cm^{-2} s^{-1} on Nov 29, i.e. by factors ≈ 60 and ≈ 55, respectively. The corresponding source X-ray luminosities were $L_{\rm x} \sim 2 \times 10^{30}$ erg s^{-1}, in quiescence, and $L_{\rm x} \sim 1 \times 10^{32}$ erg s^{-1} at the peak of both flares. In Fig. 7 we show the similar time evolution of the X-ray luminosity and of its ratio with respect to the bolometric luminosity, $L_{\rm bol}$, in the course of the two flares: in quiescence, AB Dor emits about $10^{-3} L_{\rm bol}$ at X-ray wavelengths, but during the observed flares this fraction increased by a factor 100; the total energy released, computed by simple trapezoidal integration of the contributes in the first six time segments (quiescent emission excluded), was about 6–8 $\times 10^{35}$ erg, i.e. the amount of energy bolometrically emitted by the star in about 400 sec.

4.3. 1-T analysis of MECS spectra

In order to study the flare emission only, we have performed 1-T spectral fits of the data, with the quiescent emission taken into account by including its best-fit 2-T model as a frozen background contribution. This is equivalent to consider the flare emission subtracted of the quiescent level, and allows us to derive one "effective" temperature and one emission measure of the flaring plasma, for each time segment; as we will see later (Sect. 5) this is required to analyze the flare decay. We have fitted the MECS spectra alone for several reasons: i) more time intervals can be considered, namely those were LECS data are not available; ii) 1-T models yield statistically acceptable fits to the MECS data, whereas 2-T models are required when the LECS data are included; iii) given the hard bandpass of the MECS, the fitted spectra are insensitive to the modest absorption indicated by the previous analysis, so that the number of free parameters can be reduced; iv) we can re-derive the plasma metal

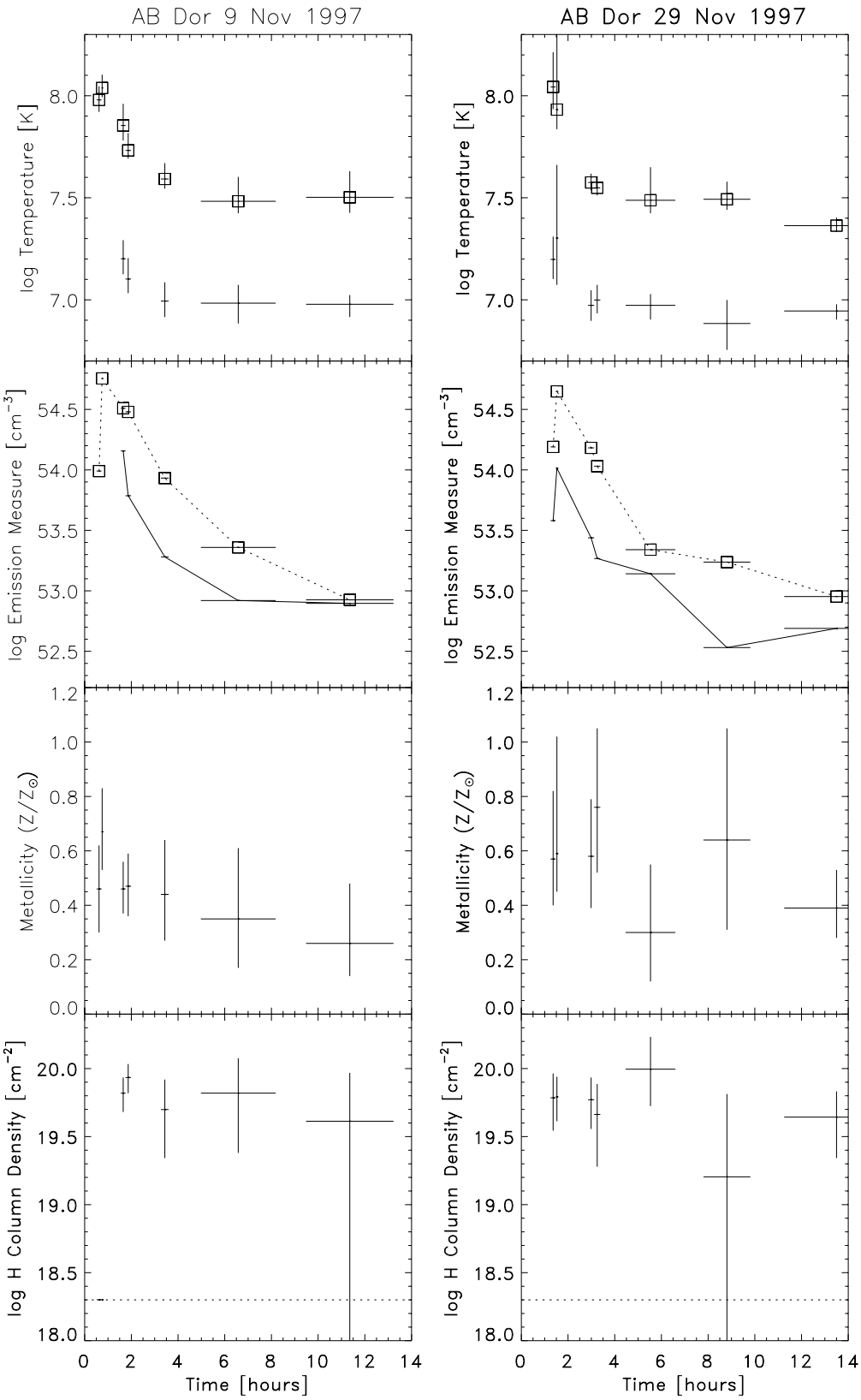

Fig. 6. Time evolution of best-fit temperatures, emission measures, metallicity, and hydrogen column density, derived by fitting LECS and MECS23 spectra of AB Dor during the 9 Nov 1997 flare (left) and the 29 Nov 1997 flare (right). The square symbols in the temperature and emission measure plots refer to the hotter thermal component. The dashed line in the H column density plots indicate the value of the ISM column density derived from EUV data (Mewe et al. 1996).

abundances, which are now essentially determined by the ratio between the Fe K line complex at 6.7 keV and the underlying continuum, given the very high plasma temperatures and the MECS bandpass.

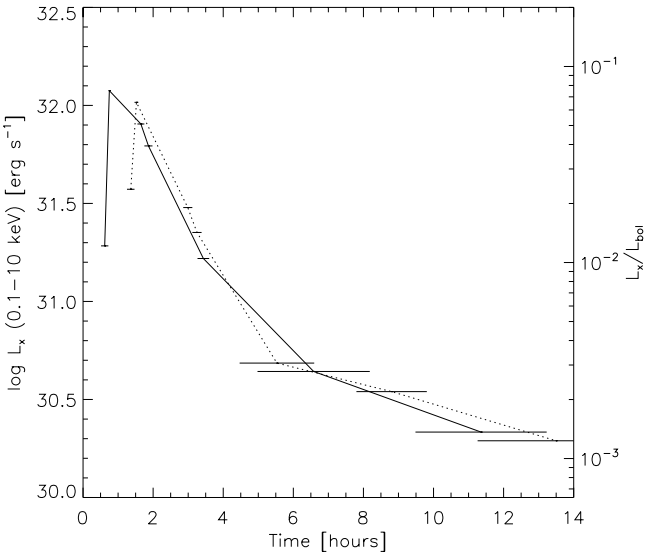

Fig. 7. Time evolution of the source X-ray luminosity (scale on the right), and of the X-ray to bolometric luminosity ratio (scale on the left), for the AB Dor flares. The solid line connects the time segments selected for the 2-T model fitting of the LECS and MECS spectra taken on Nov 9, while the dotted line marks the Nov 29 flare.

We have chosen 9 time segments for the Nov 9 observation, and 10 segments for the Nov 29 observation, which are shown, in part, in Fig. 2; note that some of the time segments previously used have been split. In Table 2 we have reported the central time of each segment, the average MECS23 count rate, which will be used for the analysis of the flare decay (Sect. 5), and the results of the 1-T model fitting. For ease of comparison with the flare characteristics, the quiescent MECS spectrum (labeled q) has been also re-fitted with a pure 1-T model.

Note that, on Nov 9, the maximum temperature and emission measure are both found in segment #2, while on Nov 29 the temperature peaks in segment #2, and the emission measure in segment #4. The best-fit values of the metal abundance are in agreement with those indicated by the 2-T modeling of the joint LECS and MECS spectra, and are more robust because no cross-talk with the H column density is present in this case. We conclude that the variation of the metal abundance during both flares, if any, was smaller than a factor ~ 3: a larger variation, if occurred, would have been detected by our analysis, at the 90% confidence level.

5. Flare decay analysis

We have analyzed the flare decays with the approach developed by Reale et al. (1997), which allows deriving properties of the flaring region, including its size, and provides us with a sensible diagnostic of sustained heating during the decay itself.

The main assumptions of the method are the following: the flare occurs in a single coronal loop with constant geometry, where the plasma is magnetically-confined. The method is calibrated, for a given observation instrument, by means of simulations of flaring loops with a detailed hydrodynamic code (Peres et al. 1982; Betta et al. 1997). In Appendix B we describe the method in greater detail, and we give the formulas, specifically derived for the case of SAX/MECS observations, required to estimate the semi-length of the flaring loop, L, from the following observational quantities: the light curve e-folding decay time, $\tau_{\rm LC}$, the slope of the decay path in the density–temperature diagram, ζ, and the maximum plasma temperature, $T_{\rm obs}$. The formulas are those appropriate for the case of loops smaller than the pressure scale height at the flare maximum temperature, condition which has to be verified a posteriori, for consistency.

The method works best if the decay is observed from the emission measure peak down to the time at which the source count rate is $\sim 10\%$ of the peak value. By considering, for each flare, five time segments (# 3–7 on Nov 9, and # 4–8 on Nov 29, as reported in Table 2), we have derived: i) decay times $\tau_{\rm LC}$ (Fig. 8) of 64 ± 2 min and 57 ± 2 min on Nov 9 and Nov 29, respectively; ii) slopes ζ of the decay in the $\log\sqrt{EM} - \log T$ diagram (Fig. 8) equal to 0.53 ± 0.19 and 0.88 ± 0.20; iii) plasma maximum temperatures (Eq. B.2) $T_{\rm max} \approx 1.7 \times 10^8$ K and 1.4×10^8 K.

Then, we have computed (Eq. B.3) the values of the ratio between $\tau_{\rm LC}$ and the loop thermodynamic cooling time, $\tau_{\rm th}$

Table 2. One-temperature model fitting[a] of the MECS spectra.

Bin[b] ID	$t_{\rm bin}^{\rm c}$ hours	Rate cts/s	$Z/Z_\odot$	T 10^6 K	$EM/10^{52}$ cm^{-3}	$\chi^2_{\rm r}$/dof
			9 Nov			
1	0.62	4.8	$0.5^{+0.2}_{-0.2}$	107^{+28}_{-19}	88^{+5}_{-5}	0.8/56
2	0.75	29.6	$0.7^{+0.2}_{-0.2}$	114^{+20}_{-16}	550^{+32}_{-27}	0.8/56
3	1.60	17.4	$0.4^{+0.1}_{-0.1}$	58^{+6}_{-6}	414^{+21}_{-24}	0.9/56
4	1.69	15.6	$0.4^{+0.1}_{-0.1}$	52^{+7}_{-3}	382^{+21}_{-24}	0.9/55
5	1.80	13.4	$0.5^{+0.2}_{-0.1}$	48^{+5}_{-3}	345^{+21}_{-19}	0.9/43
6	1.92	12.1	$0.5^{+0.2}_{-0.1}$	48^{+5}_{-5}	302^{+19}_{-19}	1.2/43
7	3.43	3.0	$0.4^{+0.2}_{-0.2}$	36^{+5}_{-2}	88^{+8}_{-5}	0.9/43
f	6.58	0.7	$0.3^{+0.3}_{-0.2}$	26^{+3}_{-2}	29^{+5}_{-3}	0.6/38
q	11.36	0.3	$0.4^{+0.2}_{-0.2}$	26^{+1}_{-2}	12^{+2}_{-1}	0.8/37
			29 Nov			
1	1.34	5.2	$0.5^{+0.2}_{-0.2}$	81^{+20}_{-14}	104^{+8}_{-8}	0.7/43
2	1.44	18.8	$0.5^{+0.2}_{-0.2}$	100^{+30}_{-19}	366^{+24}_{-24}	1.0/41
3	1.50	22.9	$0.5^{+0.2}_{-0.1}$	78^{+13}_{-10}	476^{+29}_{-27}	1.0/49
4	1.55	24.3	$0.6^{+0.2}_{-0.2}$	68^{+10}_{-8}	516^{+32}_{-32}	0.9/49
5	2.82	6.7	$0.6^{+0.4}_{-0.3}$	42^{+7}_{-6}	219^{+29}_{-24}	0.6/44
6	2.99	5.2	$0.5^{+0.2}_{-0.2}$	39^{+3}_{-3}	144^{+11}_{-11}	1.0/43
7	3.25	3.9	$0.8^{+0.3}_{-0.3}$	34^{+3}_{-2}	107^{+11}_{-8}	0.6/43
8	3.53	3.2	$0.5^{+0.3}_{-0.2}$	35^{+3}_{-3}	118^{+13}_{-8}	0.8/44
9	4.84	0.8	$0.5^{+0.4}_{-0.3}$	29^{+3}_{-2}	29^{+5}_{-4}	0.5/44
q	24.83	0.2	$0.5^{+0.3}_{-0.2}$	21^{+1}_{-1}	10^{+2}_{-1}	0.9/41

[a] Fixed 2-T quiescent emission model added to the fitted isothermal component in all cases, except for bins q. The 68% joint confidence errors have been computed with the criterium $\chi^2 < \chi^2_{min} + 3.5$, for the three interesting parameters $Z/Z_\odot$, T and EM.

[b] The time segments identified with a letter are the same already reported in Tab. 1.

[c] Central value of time bin, from the beginning of the observation.

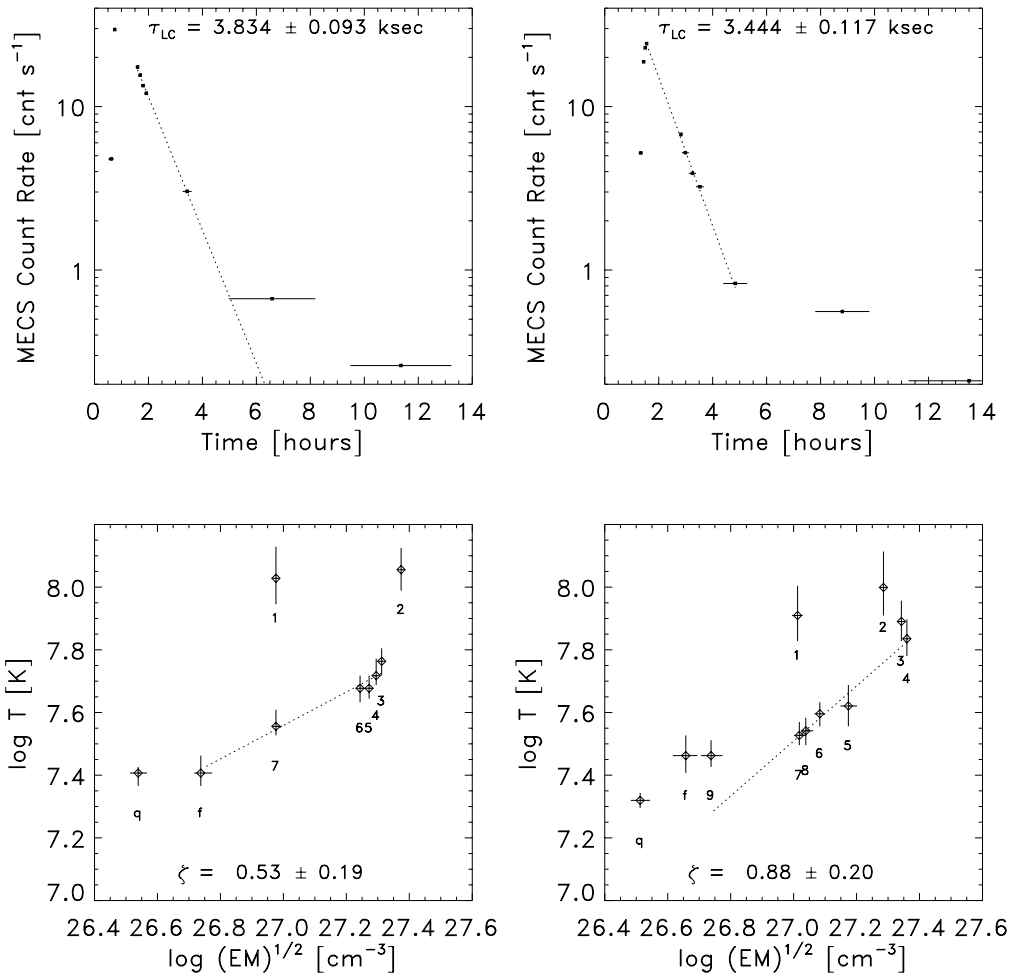

Fig. 8. MECS light curve with best-fit exponential decay law (top), and flare evolution in the $\log T_{\rm obs}$ vs. $\log \sqrt{EM}$ diagram with best-fit linear regression curve (bottom), for the Nov 9 (right) and Nov 29 (left) observations.

(Serio et al. 1991): we have obtained $\tau_{\rm LC}/\tau_{\rm th}$ = 3.8 on Nov 9, and 2.3 on Nov 29, indicating that the decay of both flares is driven by the time scale of the heating process, rather than by the much shorter thermodynamic cooling time of the plasma; the estimated heating time scales are $\tau_{\rm H} \gtrsim 4\tau_{\rm th} \sim 4000$ s on Nov 9, and $\tau_{\rm H} \sim 2\tau_{\rm th} \sim 3000$ s on Nov 29.

Finally, the loop semi-lengths (Eq. B.4) resulted $L = 3.5 \pm 1.3 \times 10^{10}$ cm, and $L = 4.9 \pm 1.8 \times 10^{10}$ cm, on the two dates, corresponding to $0.5R_*$ and $0.7R_*$, respectively. The implied loop heights ($2L/\pi$, assuming a semi-circular geometry and vertical loops) are 0.3–0.4 times the stellar radius, and 0.02–0.03 times the pressure scale height of the plasma at the flare peak. The loops are also smaller (0.1–0.2 times) than the pressure scale height of the plasma in quiescent state, where $T_{\rm max} \approx 25$ MK.

From the size of the loops we can estimate an *average* plasma density:

$$n_{\rm e} = \left(\frac{EM}{0.8V}\right)^{1/2} \tag{2}$$

where EM is the emission measure derived from the fit, 0.8 is the ratio of H to electron number densities, and V the loop volume. Assuming $\beta = 0.1$–0.3 for the ratio between the radius of the loop cross-section and its semi-length (a typical value for solar coronal loops; Golub et al. 1980), $V = 2\pi L^3\beta^2 = 0.3$–$2.4 \times 10^{31}$ cm^3 and 0.7–6.7 $\times 10^{31}$ cm^3, for the Nov 9 and Nov 29 loop, respectively. The fitting results at the flare peak then yield $n_{\rm e} = 16.0$–5.4×10^{11} cm^{-3} and 9.0–3.1 $\times 10^{11}$ cm^{-3}, in the two cases, and the corresponding pressures $p_{\rm e} = 2n_{\rm e}kT_{\rm obs} =$ 5.0–1.7 $\times 10^4$ and 1.7–0.8 $\times 10^4$ dyne cm^{-2}.

As a consistency check, we can compare the above plasma pressures with those computed in the assumption of a loop in hydrostatic conditions[2]. In that case, the plasma pressure, the temperature at the loop top, and the loop semi-length are linked by the Rosner et al. (1978) scaling law:

$$T_{\rm max} = 1.4 \times 10^3 \, (p_0 \, L)^{1/3} \, {\rm K} \tag{3}$$

from which we derive, at the time of the temperature peak, $p_0 = 5 \times 10^4$ dyne cm^{-2}, on Nov 9, and 2×10^4 dyne cm^{-2}, on Nov 29. The similarity of p_0 and $p_{\rm e}$, for the case $\beta = 0.1$, would imply that the plasma at the flare peak is not far from hydrostatic equilibrium, i.e. the loop is filled almost completely with plasma evaporated from the chromosphere, as a consequence of the heating. Larger values of β imply that the loop would be only partially filled with hot plasma at the flare peak.

[2] Since the loop is smaller than the pressure scale height, the plasma is essentially isobaric

A reasonable estimate of the energy deposition rate can be obtained from the plasma maximum temperature at the flare peak, through the Rosner et al. (1978) scaling law[3],

$$E_{\rm H} \simeq 10^{-6}\, T_{\rm max}^{7/2}\, L^{-2}\ {\rm erg\ cm^{-3}\ s^{-1}}. \quad (4)$$

The maximum heating rate per unit volume, $E_{\rm H}$, assumed uniform along the loop, results of ~ 47 and ~ 14 erg cm^{-3} s^{-1}, for the Nov 9 and the Nov 29 flare, respectively; the difference by a factor ~ 3 is due both to the higher plasma temperature of the Nov 9 flare, and to the smaller size of the loop involved. The total heating rate, $E_{\rm H}V \propto T_{\rm max}^{3.5}\, L\beta^2$, is therefore similar for two flares, and comprised in the range $\approx 10^{32}$–10^{33} erg s^{-1}, depending on the value of β. If we assume that the heating was constant during the rise phases, which lasted about 15 min ($= \tau_{\rm rise}$)[4], and then it decayed exponentially, with an e-folding time equal to $\tau_{\rm H}$, the total energy released during the flares can be estimated as $E_{\rm tot} = E_{\rm H} V \tau_{\rm tot}$, where $\tau_{\rm tot}$ is the sum of the rise time and of the heating decay time: for $\beta = 0.1$, the computed values are $E_{\rm tot} \sim 6 \times 10^{35}$ erg, on Nov 9, and $\sim 4 \times 10^{35}$ erg, on Nov 29, or about an order of magnitude larger if $\beta = 0.3$. Since the total energy deposited must exceed the energy lost by radiation in X-rays (Sect. 4.2), we conclude that $\beta \gtrsim 0.2$.

6. Discussion

6.1. Unsteady, quiescent AB Dor

The putatively quiescent X-ray emission of AB Dor is characterized by significant low-level variability, but no clear rotational modulation appears from inspection of the X-ray light curve (Fig. 4), or at least, any such effect is not as evident as the steady sinusoidal light curve observed in optical. In fact, only by means of a detailed periodogram analysis of ROSAT observations, taken over a period of 5 years, Kürster et al. (1997) were able to assess that some fraction of the observed emission, in the 0.1-2.4 keV band, was rotationally-modulated: in their case, the variability attributed to rotational modulation was $\pm$ 5–13% during a long (46 ksec) pointed observation, and $\pm$ 19% in the ROSAT All-Sky Survey data.

We have found similar levels of variability in the two energy bands considered here, namely a scatter (standard deviation) of 21% around the mean count rate in the 0.1–1.8 keV band, and of 24% in the 1.8–8 keV band, indicating that the variability is not preferentially associated to plasma at a given temperature. This result differs from the early one, based on EXOSAT data (Collier-Cameron et al. 1988), where a 30% modulation of the X-ray emission was found only in the low-energy band 0.05–2 keV, and interpreted as due to a class of relatively cool ($T < 6 \times 10^6$ K) low-lying coronal loops. On the other hand, the average X-ray flux during the SAX observations, $f_{\rm x}$ = 7–8 $\times$ 10^{-11} erg cm^{-2} s^{-1}, is about twice the value derived from the EXOSAT data, but similar to the one estimated by Vilhu & Linsky (1987) from *Einstein*/HRI data (after correcting for the different energy band).

Our interpretation of the above results is that most of the "quiescent" variability originates from low-level, steady flaring activity, occurring over a large fraction of the stellar surface, on spatial scales smaller than the stellar radius, and on time scales much shorter than the rotation period; such an activity may easily hide any rotational modulation that might be due to a large-scale spatial inhomogeneity of the corona.

Such a scenario is consistent with the bimodal profile of the transition region C IV resonance line, observed by Vilhu et al. (1998) with the Goddard High-Resolution Spectrograph on the Hubble Space Telescope. The *quiescent* profile includes a narrow (FWHM = 70 km s^{-1}) and a broad (FWHM = 330 km s^{-1}) component, which were interpreted in terms of random multiple velocities due to transient events in the transition region, and to (micro-)flaring activity, respectively; during some impulsive bursts, lasting 2–5 min in total, an additional very broad (FWHM = 800 km s^{-1}) and blue-shifted (-190 km s^{-1}) component appeared, likely due to heating and subsequent evaporation of chromospheric plasma.

A final piece of information is provided by the relatively high temperature of the coronal plasma in quiescent condition. In fact, we have found that much of the emission measure (8–9 $\times 10^{52}$ cm^{-3}) is at temperatures of 20–30 MK, and a smaller but comparable amount is at temperatures $\lesssim 10$ MK. Our results are consistent with the former ones by Rucinski et al. (1995) and by Mewe et al. (1996), except that the total emission measure we have derived ($EM \sim 1.4 \times 10^{53}$ cm^{-3}) is about twice the value inferred from the analysis of simultaneous EUVE and ASCA data (Mewe et al. 1996).

A direct implication of such high plasma temperatures, coupled with a surface gravity 0.76 times the solar one, is a hydrostatic pressure scale height of the order of 10^{11} cm, i.e. comparable to if not larger than the stellar radius, and a thermal energy more than 10 times larger than the gravitational energy, at the stellar surface. The consequences are that (i) the closed magnetic structures will be filled with hot plasma up to heights of one stellar radius above the photosphere, (ii) the maximum coronal volume available (assuming complete surface coverage) is of the order of 10^{34} cm^3, (iii) the total emission measure, derived from our analysis, implies *average* plasma densities $\approx 3 \times 10^9$ cm^{-3}, or more if only a fraction of the available volume is occupied by the hot plasma.

6.2. Coronal metallicity

The SAX X-ray spectra suggest a coronal metallicity about half solar, confirming – at least qualitatively – the significant underabundance with respect to the photospheric composition, already reported in previous studies based on EUVE and ASCA data (Mewe et al. 1996; Ortolani et al. 1998). From a quantitative point of view, our results appear marginally consistent with the EUVE and ASCA ones: the iron abundance reported by Mewe et al. (1996), 0.23 ± 0.02 solar, rests at the lower boundary of the range allowed by our data for the global metallicity, but all the other element abundances (O, Ne, Mg, Si, S) are rel-

[3] This is due to the high efficiency of the thermal conduction in corona (Reale et al. 1999)

[4] The rise phase is here defined as the time interval from the beginning of the flare to the temperature peak; in our case, it was estimated as the total length of the time segments 1 and 2 in Table 2

atively larger than the iron one (from 0.35 solar for Si, to 1.2 solar for Ne).

No large and systematic variation of the metal abundance has been detected during the flares observed with *Beppo*SAX. Given the quality of our data, if any enhancement of the metallicity occurred, it was certainly smaller than a factor 3. A different behavior has been reported for flares on other stars, e.g. Algol (Ottmann & Schmitt 1996; Favata & Schmitt 1999), the RS CVn-like binaries II Peg (Mewe et al. 1997) and UX Ari (Güdel et al. 1999), the weak-lined T Tauri star V773 Tau (Tsuboi et al. 1998), and the dMe star EV Lac (Favata et al. 2000). In all these cases, the metallicity increased by a factor 3–5 near the flare peak, and then it decayed toward the pre-flare value (except UX Ari, where the flare decay was not visible). Abundance variations of a factor ~ 3 were also indicated by the analysis of two flares on AB Dor observed by ASCA (Ortolani et al. 1998), albeit the variations were only marginally significant.

6.3. Circumstellar absorption?

The amount of intervening absorption, indicated by the soft energy part of the LECS spectra, turns out to be much larger than derived from the EUV spectra ($N_{\rm H}$ = 2–8 $\times 10^{19}$ cm^{-2} vs. $2.0 \pm 0.5 \times 10^{18}$ cm^{-2}), but consistent with the value (1.7×10^{19} cm^{-2}) reported by Schmitt et al. (1997), based on ROSAT data. Similar discrepancies have been noted in other cases (Tagliaferri et al. 1999; Pallavicini et al. 1999; Rodonò et al. 1999; Favata & Schmitt 1999; Covino et al. 1999), with the H column densities obtained by fitting X-ray spectra from *Beppo*SAX systematically higher than expected. It has been suggested by Rodonò et al. (1999) that the extra-absorption may be due to the presence of neutral hydrogen in the circumstellar environment. This suggestion appears especially appealing in the case of AB Dor, which is well known for its system of cool (8-9 $\times 10^3$ K) clouds, located at distances of 3–10 R_* from the rotation axis. Collier Cameron et al. (1990) have estimated total H I+H II column densities of 10^{20} cm^{-2}, and a total cross-sectional area 15–20% of the projected stellar disk area, for the 6–10 clouds visible at any time. Although these clouds may contribute to the soft X-ray absorption, the high $N_{\rm H}$ values found for *virtually all* active coronal sources observed by *Beppo*SAX so far, make this interpretation unlikely. The alternative possibilities which come to mind involve uncertainties in the calibration of the instrument response at low energies, or inadequacies of the fitting model revealed by the broad spectral band of *Beppo*SAX.

A separate issue is whether the column absorption may have varied during the flares. Enhancements of the hydrogen column density, associated with large flaring events, have been already observed in the past on Prox Cen (Haisch et al. 1983), V773 Tau (Tsuboi et al. 1998), and Algol (Favata & Schmitt 1999), and often interpreted as due to a coronal mass ejection. No such behavior is evident in our case, but – on the other hand – solar observations show that coronal mass ejections and flares are not always physically related one to another (Golub & Pasachoff 1997).

6.4. Hot, dense flaring plasma

What makes the present AB Dor flares really exceptional are, of course, the high plasma temperatures and emission measures ($T \gtrsim 100$ MK, $EM \approx 5 \times 10^{54}$ cm^{-3}), and the peak X-ray luminosities ($L_{\rm x} \sim 10^{32}$ erg s^{-1}, $L_{\rm x}/L_{\rm bol} \lesssim 0.1$). In fact, emission at energies up to ~ 40 keV has been detected with the *Beppo*SAX HPGSPC and PDS detectors, as discussed more extensively in Pallavicini et al. (in preparation).

On the other hand, some characteristics of these flares make them qualitatively similar to many solar flares, in spite of the very different energetics: the relatively short rise time of ≈ 15 min, faster than the decay e-folding time of about one hour, and the temperature peak preceding the emission measure peak (clearly seen only on Nov 29).

The analysis of the flare decay with the method of Reale et al. (1997) provided us with evidence of sustained heating (on time scales of 50–70 min), and with estimates of the sizes of the coronal loops involved ($L \sim 3.5 \times 10^{10}$ cm on Nov 9, and $\sim 5 \times 10^{10}$ cm on Nov 29, with an aspect ratio $\beta \gtrsim 0.2$) and of the flare energetics ($E_{\rm tot} \gtrsim 10^{36}$ erg).

Such estimates are more accurate than others, based on simple approximations which assume impulsive heating and neglect any mass exchange with the chromospheric reservoir; however, we are aware that they remain somewhat model-dependent. As discussed by Schmitt (1994) and by Pallavicini (1995), alternative flare models can often reproduce the observed flare light curves and temperature decays, yielding different flare parameters. However, the results we have obtained with the method by Reale et al. (1997) provide a completely self-consistent scenario.

The prolonged heating in the decay phase is a characteristic shared with other stellar flares that have been analyzed in the same fashion, on the dMe stars AD Leo (Reale & Micela 1998) and EV Lac (Favata et al. 2000), on Algol (Favata & Schmitt 1999), and on the same AB Dor (Ortolani et al. 1998). This effect determines the observed decay e-folding time, which is $\gtrsim 4$ times longer than the free thermodynamic cooling time, on Nov 9, and ≈ 2 times longer on Nov 29. The loop lengths obtained by taking into account the sustained heating are smaller than those computed assuming a heating abruptly switched off. An estimate of the loop length in absence of sustained heating, as assumed in the classical analysis of stellar X-ray flares, could be simply obtained by equating the light curve decay time with the thermodynamic cooling time (Serio et al. 1991; Reale et al. 1997), the latter mainly driven – in our case – by the radiative losses because of the high plasma density: the result is that the lengths of both loops would be $\simeq 10^{11}$ cm, i.e. still comparable to the stellar radius and, in any case, not significantly larger than it.

The "average" plasma densities, computed from the loop sizes and the peak emission measures, are in the range 3×10^{11}–10^{12} cm^{-3}, depending on the loop aspect ratio. Such high coronal densities are common in active binaries (Dupree et al. 1993; Schrijver et al. 1995; Brickhouse & Dupree 1998), and similar

values have been estimated also for the other large flares on EV Lac and Algol, cited above.

Most of the previous X-ray flares on AB Dor, detected with *Einstein* and GINGA, showed decay times from $\lesssim 7$ min to 35 min, which were used by Vilhu et al. (1993) to estimate loop heights of the order of 10^{10} cm, and plasma densities $\simeq 10^{12}\,\mathrm{cm}^{-3}$. Intense flaring activity was observed with ASCA over a period of 11 hours, with the two largest flares separated by half a rotation period (White et al. 1996; Ortolani et al. 1998). These two flares and the present ones, observed with *Beppo*SAX, have all e-folding decay times of about one hour, but their analysis again suggests that the emission comes from high-density plasma ($n_\mathrm{e} \sim 10^{12}$ cm^{-3}) confined in coronal loops of height 2–3 $\times 10^{10}$ cm, i.e. comparable to but smaller than the stellar radius.

In other four occasions in the past, the X-ray emission from AB Dor was observed to increase by factors 2–4 on relatively long time scales, of the order of 100 min: the first two of these events were observed with EXOSAT, and interpreted by Collier Cameron et al. (1988) as flares occurring in very long (several stellar radii) coronal loop structures; however, the decay phase was not observed. The third event was detected by GINGA, but the decay time (35 min) in that case was much shorter than predicted if the flaring region were really extended (Vilhu et al. 1993). The last event of this kind was observed by ROSAT and reported by Schmitt et al. (1997), who pointed out that alternative interpretations are possible beside a flare, namely a rotational modulation effect (e.g. the rise of a large coronal structure at the stellar limb), or an intense coronal brightening.

The emerging picture is that flares on AB Dor usually occur in coronal loops which are comparable with the stellar radius but smaller than it. These structures are also smaller than the plasma pressure scale height in quiescent state, because of the relatively high coronal temperature ($T \gtrsim 10$ MK). The only (indirect) evidence of very large coronal magnetic structures, with sizes of several stellar radii, comes from the existence of circumstellar clouds trapped at distances larger than the co-rotation radius ($r_\mathrm{c} = 2.5 R_*$, at the equator). There is no evidence of flares originated from these magnetic field regions, and no clear correlation between flaring events and the intrinsic variability of the prominences has been observed so far. On the other hand, Donati et al. (1999) found that this variability is not associated with any abrupt change in the photospheric brightness or in the surface magnetic distribution, and concluded that the variability results from reorganization of field lines at coronal level.

Finally, we can estimate the magnetic field required to power the flares, while keeping the plasma in a stable magnetic loop configuration. Assuming that the flare is compact, and that the energy released is of magnetic origin, we equate the total flare energy (Sect. 5) with the difference of energy in the magnetic fields, B and B_0, before and after the flare:

$$E_\mathrm{tot} = (B^2 - B_0^2)\frac{V_\mathrm{loop}}{8\pi} \tag{5}$$

where V_loop is the loop volume. We estimate B_0 as the field required to confine the plasma at the flare peak

$$B_0 = (8\pi p_\mathrm{e})^{1/2} = (16\pi k n_\mathrm{e} T_\mathrm{obs})^{1/2} \tag{6}$$

where n_e is the average plasma density (Eq. 2). Assuming $\beta = 0.2$, we get $B_0 = 600$–800 G, and $B = 1.3$–2.4 kG. This result can be interpreted in the framework of the flare energy stored in a magnetic field configuration (e.g. a large group of spots) with a field strength of 1-2 kG, covering a volume comparable to the one of the flaring loop. Such a configuration can be attained with the strength and coverage of the photospheric magnetic fields, as derived by Donati & Collier Cameron (1997): in fact, they found that about 20% of the surface of AB Dor is covered with fields exceeding 200 G, with typical values of 500 G and peaks up to 1.5 kG, within the magnetic regions. The similarity of these field strengths with those estimated above, can be taken as a further consistency check of our analysis.

6.5. Location of the flaring loops

The visibility analysis of our flaring coronal loops, as a function of the stellar rotation phase, adds some further information to the picture above. The Nov 9 flare occurred at the rotation phase $\phi \sim 0$, while the Nov 29 flare is at $\phi \sim 0.4$, so the loops involved might rest on opposite hemispheres *if* they were located at low latitudes. However, there is no evidence of self-eclipse of the flaring loop on Nov 9, whose maximum height[5] above the surface is $H \simeq 0.3 R_*$, thus the loop is more likely located in the circumpolar region, i.e. at latitudes $> 60°$, where it would be always visible. The situation is less clear on Nov 29: the X-ray emission decayed faster than on Nov 9, and the flare evolution can be clearly traced only to $\phi \sim 0.75$, i.e. for about 35% of the rotation period, so we are not able to determine whether the flaring loop was eventually occulted, or rather the final decay phases were masked by some unrelated brightening event (note the increase of the count rate between $\phi = 0.85$ and $\phi = 1$, in Fig. 1). We conclude that, at least for the Nov 9 event, our analysis suggests the presence of a flaring coronal loop at high latitudes. Such a conclusion would be strengthened if the inclination of the rotation axis of AB Dor were larger than the assumed value of $60°$ (cf. Appendix A).

X-ray bright magnetic structures at high latitudes are not observed in the solar case, but evidence of radio bright polar structures – based on VLBI images – has been recently reported by Benz et al. (1998), for the flare star UV Ceti, and by Mutel et al. (1998), for Algol. On AB Dor other independent indications come from the Doppler imaging (Kürster et al. 1994; Unruh et al. 1995) and from the reconstruction of the magnetic field configuration (Donati & Collier-Cameron 1997; Donati et al. 1999). In particular, Unruh et al. (1995) show that two active latitudes exist: a low-latitude ($< 30°$) band with a very stable spot distribution, producing most of the photometric modulation, and a high-latitude band, centered at $\sim 60°$, which is more variable, changing on time scales of a few rotation periods. Donati & Collier Cameron (1997) also suggest that the magnetic structures in which the prominences form, must be anchored at latitudes $> 60°$. This picture is consistent with

[5] Assuming that the loop is semicircular and not tilted

the one suggested by the visibility analysis of our flares, except that the sizes of the flaring loops are much smaller than those estimated for the prominence-supporting magnetic structures ($H > 1.5R_*$).

7. Summary and conclusions

We have presented the results of two *Beppo*SAX observations of AB Dor, covering together four rotational periods of the star, during which two intense flares have been recorded, on Nov 9 and Nov 29 1997. We have analyzed both these flares and the following quiescent phase, with the aim to characterize the coronal X-ray emitting regions.

The quiescent emission shows evidence of significant low-amplitude variability, suggesting continuous low-level flaring activity in the corona of AB Dor. A large fraction of the total emission measure ($\sim 10^{53}$ cm^{-3}) of the plasma is at temperatures > 10 MK, implying volume-averaged plasma densities $> 10^9$ cm^{-3}. The coronal metal abundance has been confirmed to be lower ($Z \sim 0.3$–0.5) than the (solar) photospheric one. The hydrogen column density, $N_{\rm H} \sim 4 \times 10^{19}$ cm^{-2}, appears to be a factor $\gtrsim 20$ larger than previously determined from EUV spectra, but in line with the high values consistently found for stellar coronae observed with *Beppo*SAX.

During both flares, the X-ray luminosity of AB Dor increased by a factor 100 in less than 20 minutes, and it decayed with an initial e-folding time of about one hour. In the case of the first flare, the quiescent level was reached again after about 12 hours, i.e. in a time about equal to the star's rotation period, but no self-eclipse of the flaring X-ray emission was observed, suggesting – at least for this event – that the flaring coronal loop is located in the circumpolar region. The second flare decayed slightly faster, so no clear hint on the location of the flaring loop can be derived from the light curve.

Spectral fits of the MECS and LECS data with thermal models show that temperatures of the order of $\sim 10^8$ K were reached at the flare peak, with volume emission measures of $\sim 5 \times 10^{54}$ cm^{-3}. During the flares we have not detected any significant variation of either the plasma metallicity Z, within a factor 3, or of the hydrogen column density.

The analysis of the flare decay phase has allowed us to estimate the sizes of the coronal loops involved: they result 2–3 times smaller than the stellar radius, and with an aspect ratio $\beta \gtrsim 0.2$. The energy deposition during the flares occurred on times scales of 50–70 min, i.e. significantly longer than the natural thermodynamic cooling time of the plasma (20–25 min), thus determining the observed e-folding decay time of the X-ray emission.

We conclude that the observed flaring loops cannot be identified with the large magnetic structures required to support the well-known slingshot prominences inferred from high-resolution Hα observations, although they may share the same location in the high-latitude activity band of AB Dor.

Acknowledgements. The authors acknowledge partial support by Ministero dell'Università e della Ricerca Scientifica e Tecnologica, and by the Italian Space Agency.

Appendix A: determination of the stellar radius

The new Hipparcos distance of 14.9 ± 0.1 pc has brought to a revision of the former pre-main-sequence classification of AB Dor: according to several authors (Micela et al. 1997; Wichmann et al. 1998; Cutispoto 1998) AB Dor is a ZAMS star of spectral type K0–K1, but its radius appears too large for a main-sequence star, as explained in the following.

Several measurements of the projected equatorial rotational velocity of AB Dor have been reported to date, ranging from $v \sin i = 100 \pm 5$ km s^{-1} (Vilhu et al. 1987) to 85 ± 5 km s^{-1} (Collier-Cameron et al. 1988; Randich et al. 1993), with the most recent determinations clustered around 91–93 km s^{-1} (Kürster et al. 1994; Unruh et al. 1995; Donati & Collier-Cameron 1997). These latter values, combined with the photometric rotation period, yield the lower limits on the stellar radius $R \sin i = 0.92$–$0.95\ R_\odot$, i.e. larger than expected for an early-K dwarf star (Schmidt-Kaler 1986). A more reasonable value, $R \sin i = 0.86 R_\odot$, is obtained assuming $v \sin i = 85$ km s^{-1}, with an inferred inclination $i \approx 90^\circ$ (Cutispoto 1998).

However, an inclination of 60° between the rotation axis of AB Dor and the line of sight has been determined by Kürster et al. (1994) and by Unruh et al. (1995), as a by-product of two different Doppler imaging techniques. Moreover, the inclination of the orbit of the low-mass companion found by Guirado et al. (1997), computed by fitting very precise astrometric data, is 59°–71°, a range which brackets the value of 60° estimated for the inclination of the rotation axis of AB Dor itself. This inclination angle, when combined with the values of $R \sin i$ given above, would imply a stellar radius comparable to or even larger than the solar one.

An independent way of deriving the stellar radius is from the parallax and the stellar diameter, the latter estimated with the Barnes-Evans relationships (Barnes et al. 1978), involving the V-band magnitude and either the $B - V$ or the $V - R$ color. Kürster et al. (1994) show that AB Dor exhibits a secular variation of the V magnitude, which decreased from 6.76 in 1979 to 7.04 in 1989, with a variability $\Delta V \sim 0.1$ on time scales of one day, due to rotational modulation. In 1989, i.e. at the epoch of the minimum V-band brightness, Kürster et al. (1994) reported also variations of the $B - V$ and $V - R_{\rm c}$ colors in the ranges 0.82–0.85 and 0.48–0.51, respectively, in phase with $V = 6.88$–7.04, over the rotation period. Assuming a linear correlation between the V magnitude and each of the two colors, we estimate that at the epoch of the maximum brightness, when $V = 6.76$ and AB Dor could be considered the least spotted, its colors were $B - V = 0.80 \pm 0.01$ and $V - R_{\rm c} = 0.46 \pm 0.01$. In fact, these estimates are in good agreement with the values measured in 1979 by Collier Cameron (1982), and in 1981 by Rucinsky (1983).

Using the transformation from Cousins to Johnson $V - R$ colors by Bessel (1983), the Barnes et al. (1978) $V - R$ relationship yields an apparent angular diameter $\theta = 0.61 \pm 0.02$ mas, and the Hipparcos parallax implies a stellar radius of $0.98 \pm 0.04 R_\odot$. Instead, the $B - V$ color relationship yields

$\theta = 0.495 \pm 0.008$ mas and $R = 0.79 \pm 0.01 R_\odot$. The radius derived from the $V-R$ color is compatible with the upper limits based on $P_{\rm rot}$ and $v \sin i$ if $61^\circ < i < 76^\circ$ (depending on the adopted value of $v \sin i$), but it is larger than expected for a main-sequence K-type star. Instead, the radius derived from the $B-V$ color is compatible with the main-sequence classification of AB Dor, but would require $v \sin i \leq 78$ km s^{-1} for $i \leq 90^\circ$.

A possible solution is that AB Dor has not yet reached the main sequence, and hence its radius is larger than for a ZAMS star of the same spectral type. This possibility was recently investigated also by Collier Cameron & Foing (1997), and found marginally consistent with the characteristics of a star with an age of 20-30 Myr, as predicted by the evolutionary models of D'Antona & Mazzitelli (1994).

In summary, there are still large uncertainties on the radius of AB Dor ($R = 0.8$–$1.0\ R_\odot$) and on the inclination of its rotation axis ($i = 60^\circ$–90°), which need to be resolved by future observations. For the purpose of the present paper we have assumed a radius of 1.0 $R_\odot$, a mass of 0.76 $M_\odot$, and an inclination $i = 60^\circ$. At the moment, this choice appears the only one which can be reconciled with the known values of the projected rotational velocity and of the period.

Appendix B: determination of flaring loop lengths

We have analyzed the flare decay phase with the approach developed by Reale et al. (1997) and Reale & Micela (1998), in order to derive the size of the flaring stellar loop. The method is based on detailed modeling of magnetically-confined plasma in coronal loop structures with fixed geometry, using the Palermo-Harvard hydrodynamic code (Betta et al. 1997). It takes into account the effects of plasma cooling, and of possible sustained heating during the flare decay. This method has been successfully tested on a sample of solar flares observed with the Yohkoh Soft X-ray Telescope (Reale et al. 1997), and recently applied to stellar X-ray flares observed with ROSAT (Reale & Micela 1998), ASCA (Ortolani et al. 1998; Favata et al. 2000), and SAX (Favata & Schmitt 1999).

In summary, the method exploits an empirical relationship between the light curve decay time and the slope of the trajectory in a temperature vs. density diagram (or equivalently temperature vs. square root of the emission measure), which has been shown to be a tracer of the heating during the decay (Sylwester et al. 1993).

For the present study the technique has been calibrated for the *Beppo*SAX/MECS response, using the same flare hydrodynamic models as in Reale & Micela (1998).

The theoretical thermodynamic cooling time of a flaring loop, i.e. the decay time in absence of sustained heating, is given by (Serio et al. 1991):

$$\tau_{\rm th} = \alpha L / \sqrt{T_{\rm max}} \qquad \text{(B.1)}$$

where $\alpha = 3.7\ 10^{-4}\ {\rm cm^{-1} s^{-1} K^{1/2}}$, L is the loop half-length (cm), and $T_{\rm max}$ is the flare maximum temperature (K).

Since the observed emission is integrated over the total loop volume and the bandpass of the instrument is limited, the "observed" plasma temperature, T_{obs} (effective value derived from isothermal fits to the X-ray spectra), is lower than the maximum temperature, $T_{\rm max}$; the following relationship was empirically determined by comparing, for a set of loop models, the actual $T_{\rm max}$ with the temperature of the isothermal model best-fitting the synthesized loop model spectrum, folded through the MECS spectral response:

$$T_{\rm max} = 0.233\ T_{\rm obs}^{1.099}. \qquad \text{(B.2)}$$

For the specific case of flares observed with the MECS, hydrodynamic simulations of flaring loops have been used to derive the function

$$F(\zeta) = \tau_{\rm LC}/\tau_{\rm th} = c_a \exp(-\zeta/\zeta_a) + q_a \qquad \text{(B.3)}$$

$$c_a = 8.68 \pm 0.04\ \ \zeta_a = 0.59 \pm 0.03\ \ q_a = 0.3 \pm 0.1$$

where $\tau_{\rm LC}/\tau_{\rm th}$ is the ratio between the observed e-folding decay time of the light-curve and the thermodynamic cooling time (Eq. B.1), and ζ is the slope of the linear decay path in the $\log \sqrt{EM} - \log T_{\rm obs}$ diagram.

Finally, from Eq. B.1, Eq. B.2, and Eq. B.3, the loop semi-length, L, for the case of loops shorter than the local pressure scale height (at the flare peak), is given by:

$$L = \frac{\tau_{\rm LC} \sqrt{0.233\ T_{\rm obs}^{1.099}}}{\alpha F(\zeta)}\ \ 0.40 < \zeta \leq 1.7 \qquad \text{(B.4)}$$

where the e-folding decay time, $\tau_{\rm LC}$, is determined by fitting the count rate light curve with an exponential law, and the slope ζ is computed with a linear regression of $\log T_{\rm obs}$ vs. $\log \sqrt{EM}$, starting from the maximum of the emission measure to $\sim 1/10$ of this value. The range of ζ indicated in Eq. B.4, is the one allowed by the modeling for the validity of the method: for $\zeta \leq 0.4$, the flare decay is entirely driven by the sustained heating, so that the thermodynamic cooling time, $\tau_{\rm th}$, cannot be determined in a reliable way, and L does not depend any more on $\tau_{\rm LC}$; at the other extreme, no sustained heating occurs, and $\tau_{\rm LC} \sim \tau_{\rm th}$[6].

The uncertainty on the computed loop length, ΔL, is given by the sum in quadrature of a term (20%) derived from consistency checks[7], and two more terms due to propagation of errors on $\tau_{\rm LC}$ and ζ, as derived from the data:

$$\Delta L = \sqrt{(0.2L)^2 + (\Delta L_1)^2 + (\Delta L_2)^2} \qquad \text{(B.5)}$$

where

$$\Delta L_1 = \frac{L}{\tau_{\rm LC}} \Delta\tau_{\rm LC} \quad \Delta L_2 = \frac{L}{\zeta_a} \left(1 - \frac{q_a}{F(\zeta)}\right) \Delta\zeta$$

The above formulae have been derived in the assumption of negligible interstellar absorption ($N_H \sim 0$) and solar metal

[6] The equality is not strict because $\tau_{\rm LC}$ depends on the energy bandpass of the instrument.

[7] In practice, it is the standard deviation of the difference between the actual value of the loop length, in each simulation, and the value derived by applying Eq. B.4.

abundances, but the corrections are negligible provided that $N_{\rm H} \lesssim 10^{20}$ cm^{-2} (Reale & Micela 1998), and the metal abundance is $Z/Z_{\odot} > 0.1$.

Finally, the heating e-folding time is directly linked to the value of the slope ζ (Reale et al. 1997), and can be estimated as follows: $\tau_{\rm H} \sim 0$ for $\zeta \gtrsim 1.4$, $\tau_{\rm H} \sim \tau_{\rm th}$ for $1 \lesssim \zeta \lesssim 1.4$, $\tau_{\rm H} \sim 2\tau_{\rm th}$ for $0.6 \lesssim \zeta \lesssim 1$, and $\tau_{\rm H} \gtrsim 4\tau_{\rm th}$ for $\zeta \lesssim 0.6$.

References

Anders E., Grevesse N., 1989, Geochimica and Cosmochimica Acta 53, 157
Arnaud M., Raymond J., 1992, ApJ 398, 394
Barnes T.G., Evans D.S., Moffett T.J., 1978, MNRAS 183, 285
Benz A.O., Conway J., Gudel M., 1998, A&A 331, 596
Bessell M.S., 1983, PASP 95, 480
Betta R., Peres G., Reale R., Serio S., 1997, A&AS 122, 585
Brickhouse N.S., Dupree A.K., 1998, ApJ 502, 918
Collier-Cameron A., 1982, MNRAS 200, 489
Collier-Cameron A., 1995, MNRAS 275, 534
Collier-Cameron A., Robinson R.D., 1989a, MNRAS 236, 57
Collier-Cameron A., Robinson R.D., 1989b, MNRAS 238, 657
Collier-Cameron A., Unruh Y.C., 1994, MNRAS 269, 814
Collier-Cameron A., Foing B.H., 1997, Observatory 117, 218
Collier-Cameron A., Bedford D.K., Rucinski S.M., Vilhu O., White N.E., 1988, MNRAS 231, 131
Collier-Cameron A., Duncan D.K., Ehrenfreund P., et al., 1990, MNRAS 247, 415
Covino S., Tagliaferri G., Pallavicini R., Mewe R., Poretti E., 1999, A&A submitted
Cutispoto G., 1998, A&AS 131, 321
D'Antona F., Mazzitelli I., 1994, ApJS 90, 467
Donati J.F., Collier-Cameron A., 1997, MNRAS 291, 1
Donati J.F., Collier-Cameron A., Hussain G. A.J., Semel M., 1999, MNRAS 302, 437
Dupree A.K., Brickhouse N.S., Doschek G.A., Green J.C., Raymond J.C., 1993, ApJ 418, L41
ESA, 1997, In: European Space Agency SP-1200 (1997)
Favata F., Schmitt J.H.M.M., 1999, A&A 350, 900
Favata F., Maggio A., Peres G., Sciortino S., 1997, A&A 326, 1013
Favata F., Reale F., Micela G., et al., 2000, A&A 353, 987
Flower P.J., 1996, ApJ 469, 355
Gehrels N., 1986, ApJ 303, 336
Golub L., Pasachoff J.M., 1997, The Solar Corona. Cambridge University Press
Golub L., Maxson C., Rosner R., Vaiana G.S., Serio S., 1980, ApJ 238, 343
Güdel M., Linsky J.L., Brown A., Nagase F., 1999, ApJ 511, 405
Guirado J.C., Reynolds J.E., Lestrade J.F., et al., 1997, ApJ 490, 835
Haisch B.M., Linsky J.L., Bornmann P.L., et al., 1983, ApJ 267, 280
Innis J.L., Coates D.W., Thompson K., Robinson R.D., 1985, Proc. Astron. Soc. Australia 6, 156
Innis J.L., Thompson K., Coates D.W., Evans T.L., 1988, MNRAS 235, 1411
Kürster M., Schmitt J.H. M.M., Cutispoto G., 1994, A&A 289, 899
Kürster M., Schmitt J.H.M.M., Cutispoto G., Dennerl K., 1997, A&A 320, 831
Lampton M., Margon B., Bowyer S., 1976, ApJ 208, 177
Lim J., 1993, ApJ 405, L33
Mewe R., Gronenschild E., van den Oord G., 1985, A&AS 62, 197
Mewe R., Kaastra J.S., White S.M., Pallavicini R., 1996, A&A 315, 170
Mewe R., Kaastra J., van den Oord G., Vink J., Tawara Y., 1997, A&A 320, 147
Mewe R., Lemen J., van den Oord G., 1986, A&AS 65, 511
Micela G., Favata F., Sciortino S., 1997, A&A 326, 221
Mutel R.L., Molnar L.A., Waltman E.B., Ghigo F.D., 1998, ApJ 507, 371
Ortolani A., Pallavicini R., Maggio A., Reale F., White S.M., 1998, In: ASP Conf. Ser. 154: Tenth Cambridge Workshop on Cool Stars, Stellar Systems, and the Sun. p. 1532
Ottmann R., Schmitt J., 1996, A&A 307, 813
Pakull M.W., 1981, A&A 104, 33
Pallavicini R., 1995, In: Greiner J., Duerbeck H.W., Gershberg R.E. (eds.) Flares and Flashes. Proc. IAU Colloquium No. 151, Lecture Notes in Physics Vol. 454, p. 148
Pallavicini R., Tagliaferri G., 1999, In: Aschenbach B., Freiberg M. (eds.) Highlights of X-ray Astronomy. MPE Special Report, in press
Pallavicini R., Tagliaferri G., Maggio A., 1999, Adv. Space Res., in press
Peres G., Serio S., Vaiana G.S., Rosner R., 1982, ApJ 252, 791
Randich S., Gratton R.G., Pallavicini R., 1993, A&A 273, 194
Reale F., Betta R., Peres G., Serio S., McTiernan J., 1997, A&A 325, 782
Reale F., Micela G., 1998, A&A 334, 1028
Reale F., Peres G., Serio S., et al., 1999, ApJ submitted
Rodonò M., Pagano I., Leto G., et al., 1999, A&A 346, 811
Rosner R., Tucker W.H., Vaiana G.S., 1978, ApJ 220, 643
Rucinski S.M., 1983, A&AS 52, 281
Rucinski S.M., 1985, MNRAS 215, 591
Rucinski S.M., Mewe R., Kaastra J.S., Vilhu O., White S.M., 1995, ApJ 449, 900
Schmidt-Kaler T., 1986, In: Voigt H. (ed.) Landolt-Börnstein Numerical Data. Vol. 3B, Springer Verlag
Schmitt J.H.M.M., 1994, ApJS 90, 735
Schmitt J.H.M.M., Krautter J., Appenzeller I., et al., 1997, A&A 325, 249
Schmitt J.H.M.M., Cutispoto G., Krautter J., 1998, ApJ 500, L25
Schrijver C., Mewe R., van den Oord G., Kaastra J., 1995, A&A 302, 438
Serio S., Reale F., Jakimiec J., Sylwester B., Sylwester J., 1991, A&A 241, 197
Sylwester B., Sylwester J., Serio S., et al., 1993, A&A 267, 586
Tagliaferri G., Covino S., Cutispoto G., Pallavicini R., 1999, A&A 345, 514
Tsuboi Y., Koyama K., Murakami H., et al., 1998, ApJ 503, 894
Unruh Y.C., Collier-Cameron A., Cutispoto G., 1995, MNRAS 277, 1145
Vilhu O., 1984, A&A 133, 117
Vilhu O., Linsky J.L., 1987, PASP 99, 1071
Vilhu O., Walter F.M., 1987, ApJ 321, 958
Vilhu O., Gustafsson B., Edvardsson B., 1987, ApJ 320, 850
Vilhu O., Gustafsson B., Walter F.M., 1991, A&A 241, 167
Vilhu O., Muhli P., Huovelin J., et al., 1998, AJ 115, 1610
Vilhu O., Tsuru T., Collier-Cameron A., et al., 1993, A&A 278, 467
White S.M., Pallavicini R., Lim J., 1996, In: ASP Conf. Ser. 109: Ninth Cambridge Workshop on Cool Stars, Stellar Systems, and the Sun. p. 299
Wichmann R., Bastian U., Krautter J., Jankovics I., Rucinski S.M., 1998, MNRAS 301, L39